Mineralogical Magazine, December 2016, Vol. 80(7), pp. 1219–1232

Tetragonal Almandine-Pyrope Phase, TAPP: finally a name for it, the new mineral jeffbenite

Fabrizio Nestola[1,*], Antony D. Burnham[2,6], Luca Peruzzo[3], Leonardo Tauro[1], Matteo Alvaro[4], Michael J. Walter[2], Mickey Gunter[5], Chiara Anzolini[1] and Simon C. Kohn[2]

[1] Dipartimento di Geoscienze, Università di Padova, Via Gradenigo, 6, I-35131 Padova, Italy
[2] School of Earth Sciences, University of Bristol, Queen's Road, Bristol BS8 1RJ, UK
[3] CNR-IGG, Padova, Via Gradenigo, 6, I-35131 Padova, Italy
[4] Dipartimento di Scienze della Terra e dell'Ambiente, Università di Pavia, Via Ferrata 1, 27100, Pavia, Italy
[5] Geological Sciences, University of Idaho, 875 Perimeter MS 3022, Moscow, 83844-3022, USA
[6] Now at Research School of Earth Sciences, Australian National University, Canberra, Australia

[*Received 5 July 2015; Accepted 16 November 2016; Associate Editor: Ed Grew*]

ABSTRACT

Jeffbenite, ideally $Mg_3Al_2Si_3O_8$, previously known as tetragonal-almandine-pyrope-phase ('TAPP'), has been characterized as a new mineral from an inclusion in an alluvial diamond from São Luiz river, Juina district of Mato Grosso, Brazil. Its density is 3.576 g/cm^3 and its microhardness is ~7. Jeffbenite is uniaxial (–) with refractive indexes $\omega = 1.733(5)$ and $\varepsilon = 1.721(5)$. The crystals are in general transparent emerald green.

Its approximate chemical formula is $(Mg_{2.62}Fe^{2+}_{0.27})(Al_{1.86}Cr_{0.16})(Si_{2.82}Al_{0.18})O_{12}$ with very minor amounts of Mn, Na and Ca. Laser ablation ICP-MS showed that jeffbenite has a very low concentration of trace elements. Jeffbenite is tetragonal with space group $I\bar{4}2d$, cell edges being $a = 6.5231(1)$ and $c = 18.1756(3)$ Å. The main diffraction lines of the powder diagram are [d (in Å), intensity, *hkl*]: 2.647, 100, 2 0 4; 1.625, 44, 3 2 5; 2.881, 24, 2 1 1; 2.220, 19, 2 0 6; 1.390, 13, 4 2 4; 3.069, 11, 2 0 2; 2.056, 11, 2 2 4; 1.372, 11, 2 0 12.

The structural formula of jeffbenite can be written as $(M1)(M2)_2(M3)_2(T1)(T2)_2O_{12}$ with M1 dominated by Mg, M2 dominated by Al, M3 dominated again by Mg and both T1 and T2 almost fully occupied by Si. The two tetrahedra do not share any oxygen with each other (i.e. jeffbenite is classified as an orthosilicate).

Jeffbenite was approved as a new mineral by the IMA Commission on New Minerals and Mineral Names with the code IMA 2014-097. Its name is after Jeffrey W. Harris and Ben Harte, two world-leading scientists in diamond research. The petrological importance of jeffbenite is related to its very deep origin, which may allow its use as a pressure marker for detecting super-deep diamonds. Previous experimental work carried out on a Ti-rich jeffbenite establishes that it can be formed at 13 GPa and 1700 K as maximum *P-T* conditions.

Keywords: TAPP, jeffbenite, physical properties, pressure/temperature conditions, diamond, São Luiz river, Brazil.

Introduction

Diamonds are able to preserve high-pressure phases as inclusions because of a combination of factors: (1) the strength of the diamond structure can maintain high pressures upon exhumation to the Earth's surface, commonly up to 2 or 3 GPa (e.g. Barron *et al.*, 2008; Howell *et al.*, 2012; Angel *et al.*, 2014; Angel *et al.*, 2015*a*,*b*), and thus limit the extent to which the stability field of a mineral is overstepped; (2) solvent/catalysts such as water and silicate melt do not come into contact with the inclusions because of the impervious nature of the diamond structure, which impedes retrogressive phase transitions; (3) the rapid ascent rate of kimberlites limits the time available for inclusions to undergo phase transitions at high temperature. Consequently, for example, coesite is a commonly encountered inclusion and, unlike most occurrences in metamorphic rocks (e.g. Chopin, 1984; Parkinson, 2000; Liou *et al.*, 2012)

*E-mail: fabrizio.nestola@unipd.it
DOI: 10.1180/minmag.2016.080.059

generally shows no signs of conversion to quartz (see Angel *et al.*, 2014 and Angel *et al.*, 2015*b*). Also encountered are majorite garnets that retain a silica excess (e.g. Stachel, 2001; Harte, 2010), unlike metamorphic examples where exsolution of the pyroxene component is complete (van Roermund and Drury, 1998 and references therein).

In this paper we present a new name for the phase commonly known as 'TAPP', Tetragonal Almandine-Pyrope Phase. 'TAPP' has been reported from numerous diamonds of sublithospheric origin since its original characterization (Harris *et al.*, 1997; Bulanova *et al.*, 2010; Armstrong and Walter, 2012; Kaminsky, 2012; Zedgenizov *et al.*, 2014). It has a composition that is very close to the stoichiometry of a garnet, but it lacks Ca and its structure is tetragonal (space group $I\bar{4}2d$; Finger and Conrad, 2000). It occurs as single grains (e.g. Harris *et al.*, 1997) or as one phase of composite, polyphase inclusions (e.g. Hutchison *et al.*, 2001; Brenker *et al.*, 2002; Walter *et al.*, 2011).

Jeffbenite is named in honour of two scientists, Jeffrey W. Harris (School of Geographical and Earth Sciences, University of Glasgow, UK; b. 1940) and Ben Harte (School of Geosciences, University of Edinburgh, UK; b. 1941), whose work on diamonds, and super-deep diamonds in particular, has shaped our understanding of mantle geochemical processes for years to come. Both were authors, together with Dr. Hutchison, Dr. Light and Prof. Hursthouse, of the original structural characterization of 'TAPP' published in *Nature* (Harris *et al.*, 1997).

Here we describe the new mineral jeffbenite in terms of its physical, chemical, optical and structural properties paying special attention to its stability field. Jeffbenite was approved in February 2015 as a new mineral by the IMA Commission on New Minerals and Mineral Names with the code IMA 2014-097. The holotype is deposited at the Museum of Mineralogy of the University of Padova under the catalogue number MMP M12660.

Historical overview

The mineral now called jeffbenite was first discovered in super-deep diamonds about 23 years ago and its occurrence was reported upon by Harte and Harris (1994). At that time these authors only had electron-microprobe (EMP) analyses of small inclusions and as it had the chemical composition of a pyrope-almandine garnet they referred to it as a 'garnet'. However, they noted the exceptional composition compared with other mantle-derived garnets; it was very poor in Ca and showed no majoritic substitution. Subsequent X-ray diffraction studies of the mineral showed that jeffbenite was not a garnet and the phase was described in detail by Harris *et al.* (1997) under the name 'Tetragonal-Almandine-Pyrope-Phase', or TAPP. The TAPP phase was never submitted to IMA for mineral approval and never described in detail, probably because of its extremely rare occurrence. For example, at the time its optical and physical properties were unknown. Only a few samples have been reported so far in the literature and very rarely as single crystals suitable for proper crystallographic, optical and physical characterization.

Jeffbenite has only been found as inclusions in diamond and, with the exception of a finding in a diamond from the Kankan alluvial deposits (Guinea) (Brenker *et al.*, 2002), only from the Juina region (Brazil).

In terms of mineral association, the most common associated phase with jeffbenite appears to be ferropericlase (e.g. Harte *et al.*, 1999), but olivine, $CaSiO_3$-walstromite, $MgSiO_3$ with enstatite structure and carbonates have also been recorded as coexisting inclusions (Hutchison *et al.*, 2001; Hayman *et al.*, 2005; Bulanova *et al.*, 2010; Thomson *et al.*, 2014).

Occurrence

The type specimen of jeffbenite studied in this work occurred as an inclusion in an alluvial diamond from São Luiz river, Juina district of Mato Grosso, Brazil (11°29′ S 59°02′ W), from which it was extracted by crushing the diamond. The jeffbenite sample formed part of a composite inclusion along with a grain of omphacitic pyroxene Between jeffbenite and omphacite we found no crystallographic relationships in terms of orientation and the two phases showed no orientation relationship with their diamond host (for an example of the procedure see Nestola *et al.*, 2014*a*). Within the same diamond, an inclusion of $CaSiO_3$-walstromite was also found.

One single crystal of jeffbenite with a size 0.07 mm × 0.05 mm × 0.03 mm was used for the present investigation (Fig. 1).

Appearance, physical and optical properties

Jeffbenite cannot be described in terms of morphology as it can be found only within diamond and thus we will never know its stable morphology.

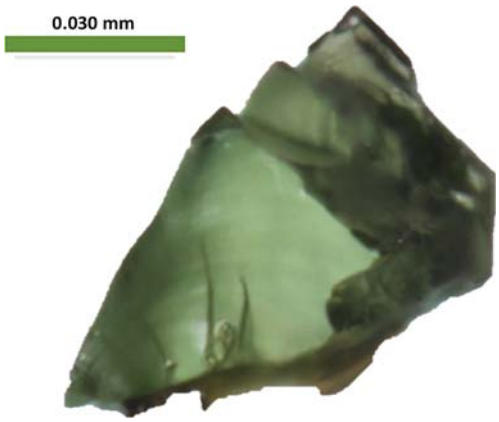

FIG. 1. The single crystal of jeffbenite studied in this work on which the crystal structure was determined together with all further physical and optical properties. The emerald green colour is characteristic for this phase.

Figure 1 only provides an indicative idea of jeffbenite shape. The crystal appears transparent and deep emerald green in colour, the streak is white and the lustre is vitreous. It is non-fluorescent and shows a micro-Vickers hardness of 1346 corresponding to a Mohs hardness of ~7. The tenacity is brittle and no cleavage was observed. The fracture is irregular. The density of jeffbenite could not be determined by classical methods due to its limited crystal size. Its calculated density using X-ray diffraction and its empirical formula provide a density 3.576 g/cm^3.

In terms of optical properties, jeffbenite is uniaxial (–), with $\omega = 1.733(5)$ and $\varepsilon = 1.721(5)$ (measured using 589 nm radiation). Its pleochroism is ε = light blue and ω = colourless. Calculation of the Gladstone-Dale relationship yields a compatibility index, $1-(K_p/K_c) = -0.011$, which is in the 'superior' category (Mandarino, 1981).

Experimental methods

Scanning electron microscopy – energy dispersive spectroscopy (EDS) and chemical mapping

In order to verify the chemical homogeneity of jeffbenite the crystal in Fig. 1 was polished and analysed by a CamScan MX3000 electron microscope equipped with a LaB_6 source, four-quadrants solid-state back-scattered electron (BSE) detector and an EDAX EDS system for micro-analysis installed at Department of Geosciences of University of Padova. The analytical conditions were: accelerating voltage of 20 kV, filament emission of ~13 nA, and working distance of 27 mm. A BSE image of jeffbenite is shown in Fig. 2. On the same polished crystal a chemical map was performed to verify the homogeneity of the following elements: Si, Mg, Al, Fe, Mn, Cr and Ca. The chemical map is shown in Fig. 3.

Single-crystal X-ray diffraction

A complete set of X-ray diffraction intensities was collected using a new prototype instrument in the Department of Geosciences at the University of Padova (Angel and Nestola, 2015). The instrument consists of an Agilent Supernova goniometer equipped with an X-ray micro-source assembled with a Pilatus 200 K Dectris detector. The micro-X-ray source, Mo$K\alpha$, operates at 50 kV and

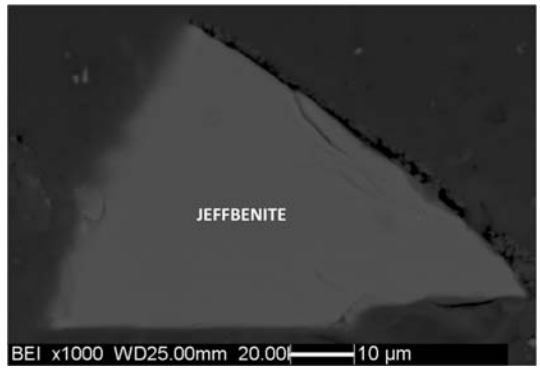

FIG. 2. A back-scattered electron image of the crystal shown in Fig. 1 after polishing. The chemical homogeneity is very evident.

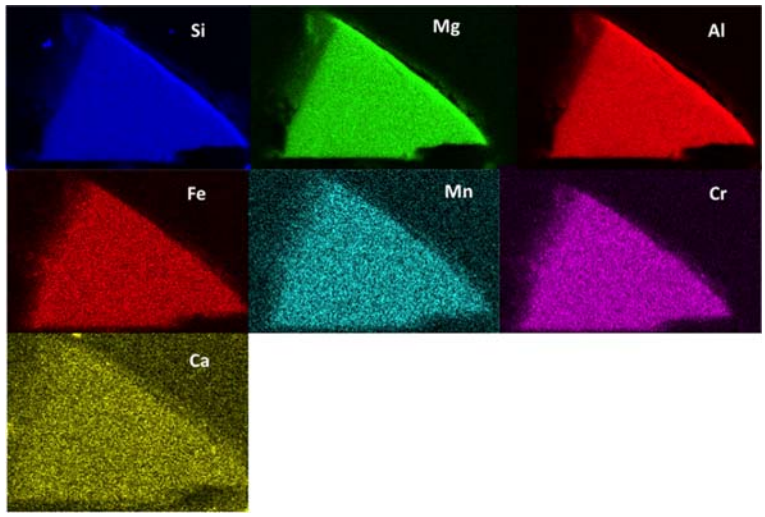

FIG. 3. Elemental distribution map of Si, Mg, Al, Fe, Mn, Cr and Ca for the jeffbenite crystal shown in Fig. 2. No further elements were mapped as the preliminary EDS results showed no other elements.

0.8 mA. The sample-to-detector distance was 68 mm. The micro source ensures a brilliance at least ten times higher than conventional sealed X-ray tubes and a beam spot of ~0.120 mm. At the same time the Pilatus 200 K detector ensures a very high sensitivity and negligible noise. The instrument is able to provide significant results on crystals of extremely small size, down to 0.01 mm. To obtain very reliable data on jeffbenite 2456 frames and 22,199 reflections were collected up to $2\theta_{max} = 80.49°$.

The redundancy was 28.9 and $F^2/\sigma(F^2) = 71.4$. The data completeness was 100% and the R_{int} (*I*4/*mmm*) was 0.039 up to maximum resolution. Data reduction was performed using *Crysalis* software (Agilent Technologies Ltd, Yarnton, UK), which corrected for Lp effects and absorption. Information relating to data collection and structure refinement, performed using *SHELX-97* (Sheldrick, 2008), is reported in Table 1. The refinement was performed using neutral scattering curves and all atoms were refined anisotropically. The starting model used was taken from Finger and Conrad (2000). Atom coordinates and U_{eq} parameters are given in Table 2. Structure factors and a crystallographic information file have been deposited with the Principal Editor of *Mineralogical Magazine* and are available from www.minersoc.org/pages/e_journals/dep_mat_mm.html. Selected bond distances are reported in Table 3. All crystal and refinement data are reported in Table 1.

Powder X-ray diffraction data were collected using the same instrument as above, which simulates a Gandolfi camera measurement mode.

TABLE 1. Crystal and refinement data for jeffbenite.

Crystal data	
Crystal size (mm)	0.070 × 0.050 × 0.030
Cell setting, space group	Tetragonal, $I\bar{4}2d$
a (Å)	6.5231(1)
c (Å)	18.1756(3)
V (Å^3)	773.38(5)
Z	4
Data collection and refinement	
Radiation, wavelength (Å)	Mo*K*α, λ = 0.71073
Temperature (K)	293
$2\theta_{max}$	80.49
Measured reflections	28,735
Total unique reflections	1218
Reflections with $F_o > 4\sigma(F_o)$	1201
R_{int}	0.0389
Range of *h*, *k*, *l*	$-11 \le h \le 11$, $-11 \le k \le 11$, $-32 \le l \le 32$
R [$F_o > 4\sigma(F_o)$]	0.0179
R (all data)	0.0184
wR (on F_o^2)	0.0551
Goof	1.048
Number of least-squares parameters	52
Maximum and minimum residual peak (*e* Å^{-3})	0.42 –0.47

TABLE 2. Crystallographic sites, Wyckoff positions, site occupancies, atom coordinates, and equivalent anisotropic displacement parameters (Å^2) for jeffbenite.*

Atom	Site	Site occupancy	*x*	*y*	*z*	U_{eq}
T1	4b	Si	0.5	0.5	0	0.00537(8)
T2	8d	$Si_{0.91}Al_{0.09}$	–0.14975(5)	0.25	0.125	0.00249(7)
M1	4a	$Mg_{0.82}Fe^{3+}_{0.12}$	0	0	0	0.0124(1)
M2	8d	$Al_{0.93}Cr_{0.08}$	0.25918(6)	0.25	0.125	0.0086(1)
M3	8c	$Mg_{0.90}Fe^{2+}_{0.075}Mn_{0.025}Na_{0.005}Ca_{0.005}$	0	0.5	–0.02302(2)	0.0106(1)
O1	16e	O	0.01873(10)	0.28028(10)	0.05749(3)	0.0079(1)
O2	16e	O	–0.26098(11)	0.03758(10)	0.10130(4)	0.0088(1)
O3	16e	O	0.43666(11)	0.29614(10)	0.04693(4)	0.0081(1)

The structural data were obtained by refining the occupancy factors at M1, M2 and M3 sites. We did not refine the site occupancy of T1 and T2 as the T1–O and T2–O bond distances do not indicate any detectable Al substituting Si (see Table 3). In addition, it is well known that by X-ray diffraction refining Al against Si does not provide any realistic number having these two elements too close atomic numbers. For the M1, M2 and M3 sites we refined their occupancies using the scattering curve of neutral iron for all three as this approach provided the best match with the EMP analysis. We obtained the following occupancy factors: M1 = 0.560, M2 = 0.527, M3 = 0.479. The calculated electrons from such factors provide an M1 + M2 + M3 sum = 40.71 against 40.50 electrons obtained using the above cation occupancies, which are only based on the EMP analysis and on a Fe^{3+}/Fe_{tot} ratio equal to 0.445 (see notes in Table 5 and/or text).
*Anisotropic displacement parameters are deposited with the cif at www.minersoc.org/pages/e_journals/dep_mat_mm.html

Data (in Å) are listed in Table 4. Unit-cell parameters were refined from the powder data using the method of Holland and Redfern (1997) on the basis of 21 unequivocally indexed reflections giving the following values: a = 6.5355(2) Å, c = 18.1576(11) Å, V = 775.56(5) Å^3, in excellent agreement with the data measured by single-crystal X-ray diffraction.

Chemical data

Chemical analyses were carried out using a CAMECA SX50 electron microprobe (wavelength-dispersive spectroscopy mode, 20 kV, 20 nA, 2 µm beam diameter) installed at CNR-IGG Institute (hosted by the Department of Geosciences of University of Padova). Standards (analyser crystal, element, emission line) used were Kakanui pyrope (New Zealand) from the Smithsonian Museum (TAP, Mg*K*α); Amelia albite (Virginia) (TAP, Na*K*α); diopside (TAP, Si*K*α; PET, Ca*K*α); Al_2O_3 (TAP, Al*K*α); $MnTiO_3$ (PET, Ti*K*α; LIF, Mn*K*α); Cr_2O_3 (LIF, Cr*K*α); Fe_2O_3 (LIF, Fe*K*α). Analytical data are given in Table 5.

Laser ablation inductively coupled plasma mass spectrometry (LA-ICP-MS) analysis was carried out using a LambdaPhysik Compex 110 Eximer 193 nm laser with a HelEX ablation chamber coupled to an Agilent 7700 series ICP-MS at the Research School of Earth Sciences in the Australian National University. The carrier gas was He–Ar, fluence was maintained at ~50 mJ and pulse rate was set to 5 Hz; two analyses were performed using a 40 µm spot size and one analysis was performed using a 100 µm spot size. The isotopes analysed were ^{23}Na, ^{29}Si, ^{89}Y, ^{90}Zr, ^{93}Nb, ^{139}La, ^{140}Ce, ^{141}Pr, ^{146}Nd, ^{147}Sm, ^{153}Eu, ^{157}Gd, ^{159}Dy, ^{163}Ho, ^{165}Er,

TABLE 3. Selected bond distances (Å) for jeffbenite.

T1–O3	1.6330(6) × 4
T2–O1	1.6591(7) × 2
T2–O2	1.6224(7) × 2
<T2–O>	1.6408
M1–O1	2.1093(2) × 4
M1–O2	2.5196(7) × 4
<M1–O>	2.3144
M2–O1	2.0012(7) × 2
M2–O2	1.9248(6) × 2
M2–O3	1.8559(7) × 2
<M2–O>	1.9273
M3–O1	2.0519(7) × 2
M3–O2	2.1249(7) × 2
M3–O3	2.0227(7) × 2
<M3–O>	2.0665

TABLE 4. Observed powder X-ray diffraction data for jeffbenite (for the observed *d*-spacings only those reflections with relative intensity >3% were reported).

Observed d-spacings (Å)	Relative intensity (%)	*h k l*	Calculated d-spacings (Å)	Calculated relative intensity (%)
6.140	4	1 0 1	6.140	2
4.126	5	1 1 2	4.113	5
3.177	9	1 0 5	3.175	12
3.069	**11**	**2 0 2**	3.070	3
2.881	**24**	**2 1 1**	2.880	17
2.647	**100**	**2 0 4**	2.650	100
2.275	8	2 1 5	2.275	2
2.220	**19**	**2 0 6**	2.220	20
2.056	**11**	**2 2 4**	2.057	4
2.013	7	3 1 2	2.012	4
1.939	5	2 1 7	1.940	5
1.871	3	3 0 5	1.878	1
1.800	5	3 2 1	1.800	4
1.705	8	3 1 6	1.705	7
1.664	7	2 1 9	1.660	4
1.625	**44**	**3 2 5**	1.618	21
1.521	6	3 3 2	1.527	2
1.484	9	3 2 7	1.484	7
1.447	6	4 1 5	1.440	1
1.390	**13**	**4 2 4**	1.390	10
1.372	**11**	**2 0 12**	1.374	6
1.318	6	4 2 6	1.314	4

Calculated *d*-spacings and relative intensities were calculated using the software *Highscore Plus* (PAnalytical) on the basis of the structural model given in Table 5.
The eight strongest reflections are given in bold.

^{166}Tm, ^{172}Yb, ^{175}Lu and ^{176}Hf. GSD-1 g glass (Jochum *et al.*, 2005) was used as the external standard and Si was used as the internal standard (nominally set to 50% SiO_2 because analyses were partially contaminated by pyroxene, see below). The results are shown in Table 6.

Micro-Raman analysis

The same crystal investigated by X-ray diffraction and microprobe was also analysed by micro-Raman spectroscopy. To the best of our knowledge this is the first micro-Raman spectrum for this phase. Raman spectra were obtained using a ThermoScientific DXR Raman microscope

TABLE 5. Chemical composition of the holotype of jeffbenite, determined by wavelength-dispersive spectroscopy.

Oxide wt.%	Range	Average
SiO_2	41.56–42.04	41.74(18)
TiO_2	0.04–0.07	0.06(1)
Al_2O_3	23.74–23.95	23.84(9)
Cr_2O_3	2.79–2.92	2.86(7)
FeO_{total}	4.55–4.62	4.59(3)
FeO	2.97–4.36	3.65(56)
Fe_2O_3	0.25–1.65	0.93(56)
MnO	0.75–0.85	0.79(4)
MgO	24.90–25.41	25.16(22)
CaO	0.08–0.10	0.09(1)
Na_2O	0.08–0.12	0.10(1)
Total	98.66–99.55	99.23

Total Fe as FeO. Fe^{3+}/Fe_{tot} was calculated using Droop's (1987) method.

TABLE 6. Trace element concentrations in jeffbenite, as determined by LA-ICP-MS. Analyses 1 and 2 were performed using a 40 μm spot size; analysis 3 was performed using a 100 μm spot size and the limit of detection (LOD) corresponding to this analysis is indicated.

	Analysis 1	Analysis 2	Analysis 3	LOD
Na_2O	5.34	2.22	3.38	–
Y	0.036	0.019	0.011	0.001
Zr	0.534	1.292	1.288	0.005
Nb	bdl	0.012	0.007	0.002
La	bdl	bdl	bdl	0.002
Ce	bdl	bdl	0.002	0.001
Pr	bdl	bdl	bdl	0.002
Nd	bdl	bdl	bdl	0.010
Sm	bdl	bdl	bdl	0.008
Eu	bdl	bdl	bdl	0.003
Gd	bdl	bdl	bdl	0.003
Tb	bdl	bdl	bdl	0.001
Dy	bdl	bdl	bdl	0.003
Ho	bdl	bdl	bdl	0.001
Er	bdl	bdl	bdl	0.004
Tm	bdl	bdl	bdl	0.002
Yb	bdl	0.007	0.004	0.003
Lu	bdl	bdl	bdl	0.002
Hf	0.030	0.046	0.048	0.003

The concentrations are provided in ppm except for Na, which is in wt.%

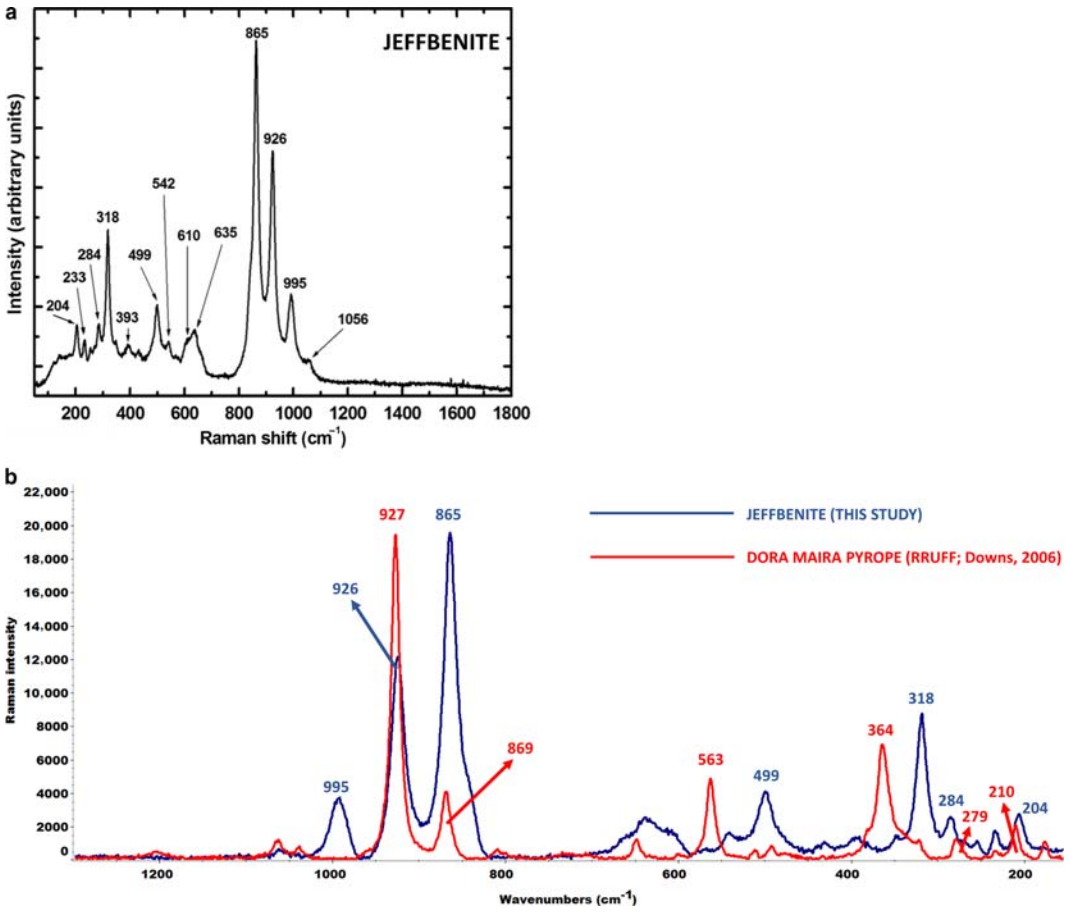

FIG. 4. Micro-Raman spectrum of jeffbenite carried out on the crystal in Fig. 1. Data were collected between 50 and 1800 cm^{-1} (see the text for more experimental details).

installed at the School of Earth Sciences of University of Bristol. A 532 nm excitation laser was used at a power of 3–5 mW to avoid any possible beam damage to the crystal; spectra were collected for ~220 s. The analysis was performed using a 50× objective with a spatial resolution of 1 μm and a spectral resolution estimated to be ~2.5 cm^{-1}. Data were collected between 50 and 1800 cm^{-1}. The Raman spectrum is shown in Fig. 4.

Results

Chemistry of jeffbenite

The empirical formula of jeffbenite, based on 12 oxygen atoms per formula unit (apfu), and on the data reported in Table 5 is the following:

$$(Mg_{0.82}Fe^{3+}_{0.12})_{\sum 0.95}(Al_{1.86}Cr_{0.16})_{\sum 2.02}(Mg_{1.80}Fe^{2+}_{0.15}Mn_{0.05}Ca_{0.01}Na_{0.01})_{\sum 2.02}(Si_{2.82}Al_{0.18})_{\sum 3.00}O_{12}.$$

No other elements were detected by EDS analysis.

The Fe^{3+}/Fe_{tot} ratio was calculated using Droop's (1987) method and for our data gives an average value of 0.18. However, the variation (see Table 5 for FeO and Fe_2O_3 wt.% calculation) is quite significant with a minimum of 0.048 and a maximum of 0.325. The only available Mössbauer measurements on the TAPP phase (McCammon *et al.*, 1997), provided much higher values of Fe^{3+}/Fe_{tot} between 0.66 and 0.74. However, a careful analysis of the chemical data on the McCammon *et al.* (1997) samples shows that using the Droop method with charge-balance considerations would give a much lower Fe^{3+}/Fe_{tot}

ratio. Their cation sum without any Fe correction and only considering the FeO_{tot} is between 7.91 and 7.95 (against the ideal value of 8), which would not require Fe^{3+} at all. We do not know the origin of this chemical discrepancy though it may lie in the low signal-to-noise ratio of the Mössbauer data. In order to obtain the best charge balance for our empirical formula we have used a value of $Fe^{3+}/Fe_{tot} = 0.445$, which is an intermediate value from our indirect determination by the Droop method and the direct Mössbauer measurement of McCammon *et al.* (1997).

The simplified formula of jeffbenite is $Mg_3Al_2Si_3O_{12}$, which requires MgO = 29.99, Al_2O_3 = 25.29, SiO_2 = 44.71 (total 100.00 wt.%).

The back-scattered electron images (Fig. 2) and X-ray maps (Fig. 3) indicate that the crystal studied is homogeneous in major-element composition and lacks exsolution features (in contrast to the specimen of Brenker *et al.*, 2002).

As reported by Armstrong and Walter (2012), 15 instances of jeffbenite have been reported in the literature up to that date. Since then, our jeffbenite sample, four inclusions found by Zegdenizov *et al.* (2014) and two more by Thomson *et al.* (2014) have been reported. Compositional data for jeffbenite were summarized by Armstrong and Walter (2012); in detail, they report six single inclusions of Ti-free and low-Fe jeffbenites, a further four composite inclusions of Ti-bearing and more ferroan jeffbenites and finally one Ti-bearing and extremely Fe-rich jeffbenite. To this list of jeffbenites, we must add our IMA approved jeffbenite, which is Ti-free and low-Fe; and a further Ti-bearing sample with very high Fe content analysed here by microprobe. This second jeffbenite has been identified in a diamond from the Collier-4 kimberlite in Brazil, and forms part of a polyphase inclusion with $(Mg,Fe)CO_3$. Electron microprobe data for our Ti-bearing and Fe-rich jeffbenite are given in Table 7. Its chemical formula is close to the jeffbenite analysed by Bulanova *et al.* (2010): see Table 8.

The concentrations of trace elements in jeffbenite (see Table 6) are low, with Zr and Hf being the most abundant of those measured, a feature also observed by Harte *et al.* (1999). The grain analysed in the present study (not the same crystal analysed by diffraction) is intergrown with a sodic pyroxene, and the three analyses all contained a contribution from this material (Na_2O varied from ~2.2–5.3%). This mixed nature of the analyses means that the SiO_2 content was assumed to be 50% (i.e. approximately halfway between jeffbenite and clinopyroxene) for processing the data, which introduces a relative uncertainty of ~10% for the bulk analyses; moreover there is no way to tell how the elements are distributed between the two phases. However, mass balance calculations

TABLE 7. Composition of Fe-rich jeffbenite and semi-quantitative analysis of coexisting magnesite in diamond RC2-7 from Collier-4 kimberlite, Brazil.

	Fe-rich jeffbenite	Magnesite
SiO_2	36.05	0.26
TiO_2	3.56	0.47
Al_2O_3	17.82	0.30
Cr_2O_3	0.01	0.03
FeO_{total}	20.12	16.51
MnO	0.37	0.62
MgO	17.99	34.05
CaO	0.04	0.42
Na_2O	0.10	0.11
K_2O	0.04	0.10
P_2O_5	0.02	–
CO_2*	–	47.12
Total	96.11	99.99

*Presence of carbonate indicated by Raman; CO_2 content inferred by difference.

TABLE 8. A comparison of the chemical compositions of Fe-rich jeffbenite, relative to 12 O per formula unit with respect to our Fe-poor jeffbenite.

Elements	(1)	(2)	(3)	(4)	(5)	(6)	(7)
Mg	2.62	2.10	1.83	1.92	2.03	2.24	2.71
Fe^{2+}	0.27	1.32	1.49	1.60	1.50	1.29	0.50
^{VI}Al	1.86	1.51	1.53	1.36	1.35	1.40	1.36
Ti	–	0.21	0.24	0.24	0.24	0.19	0.20
Si	2.91	2.86	2.72	2.84	2.81	2.87	2.78
^{IV}Al	0.09	0.14	0.28	0.16	0.19	0.13	0.22

Only the major elements are shown for comparison and all Fe was considered as Fe^{2+} even if it is known that that Fe^{3+} could be abundant. ^{IV}Al and ^{VI}Al are the aluminium in tetrahedral and octahedral coordination.
Sources: (1) this study; (2) this study; (3) Bulanova *et al.* (2010); (4) Thomson *et al.* (2014) diamond Ju5-43; (5) Thomson *et al.* (2014) diamond Ju5-102; (6) Thomson *et al.* (2014) diamond Ju5-117; (7) Ti-bearing jeffbenite reported by Armstrong and Walter (2012) averaging the jeffbenite inclusions from Harte *et al.* (1999), Kaminsky *et al.* (2001), Brenker *et al.* (2002), Hayman *et al.* (2005).

suggest that the trace-element content of jeffbenite must be in the range of zero to twice the measured concentrations. In many minerals, the rare-earth elements substitute for Ca, and the absence of Ca from jeffbenite may explain the remarkably low trace-element content.

Micro-Raman spectroscopy

The micro-Raman spectrum collected of jeffbenite is shown in Fig. 4*a*. The five main peaks, in order of decreasing intensity, are (in cm^{-1}): 865, 926, 318, 995 and 499. Lower intensity peaks are evident in the 540–640 cm^{-1} region, one peak is centred at 393 cm^{-1}, and three further peaks occur in the 200–300 cm^{-1} region. As we have no Raman spectrum of previous jeffbenites, we can only compare it with a chemically similar mineral like pyrope. Based on the work of Kolesov and Geiger (1998) on pyrope $Mg_3Al_2Si_3O_{12}$, we may divide the spectrum of jeffbenite into three main regions: (1) the 850–1060 cm^{-1} region is assigned to (Si–O) stretching modes; (2) the 490–640 cm^{-1} region is assigned to SiO_4 bending modes; (3) the 300–400 cm^{-1} region is typical of rotational modes of SiO_4^{4-} groups.

Peaks at <300 cm^{-1} may be assigned to the translational SiO_4^{4-} modes (i.e. 204 and 233 cm^{-1}) and to Mg–O vibrations (i.e. 284 cm^{-1}). The Raman spectrum of jeffbenite is distinctive and unlikely to be mistaken for other minerals.

In Fig. 4*b* we compared the Raman spectra of jeffbenite with that of pyrope from Dora Maira (Italy) and those selected from the RRUFF Raman database (Lafuente *et al.*, 2006; reference RRUFF number: R070637): in the spectra we can observe that a certain degree of overlapping is evident for peaks at 926–927, 865–869, 279–284 and 204–210 cm^{-1}. However, two important peaks of pyrope at 364 and 564 cm^{-1} are totally absent in jeffbenite and, on the contrary, the intense peak at 995 cm^{-1} is absent in pyrope. Therefore, jeffbenite can be identified confidently with respect to pyrope and any other minerals in the absence of XRD data (e.g. as part of composite inclusions).

The crystal structure of jeffbenite

The first crystallographic report for jeffbenite was published by Harris *et al.* (1997) and the same crystal studied in that work was then re-investigated by Finger and Conrad (2000). The necessity to reinvestigate jeffbenite by Finger and Conrad (2000) originated mainly because of some debate about the cation occupancies; Harris *et al.* (1997) had proposed some cation vacancies at the tetrahedral sites, which was not confirmed by Finger and Conrad (2000).

However, the structural models proposed in the two studies were nearly identical. The crystal structure of jeffbenite (Fig. 5) comprises five different cation positions. For comparison with

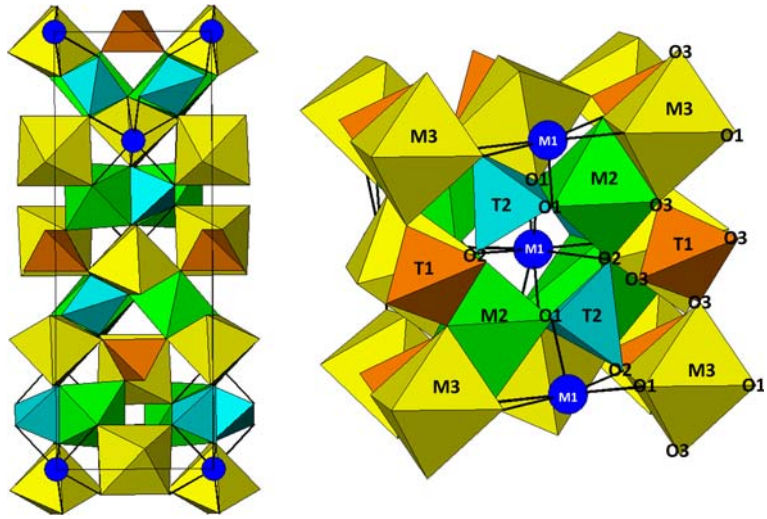

FIG. 5. Crystal structure of jeffbenite viewed perpendicular to *c* (left) and along a closed direction to the *c* axis (right) to better visualize the M1 site with the M1–O bonds.

Harris *et al.* (1997) and Finger and Conrad (2000) we used their same nomenclature: T1 and T2 are two symmetrically independent tetrahedral sites, M2 and M3 are two significantly different octahedral sites, the M1 site is represented by a capped tetrahedron.

The general formula could be (M1) $(M2)_2(M3)_2(T1)(T2)_2O_{12}$ with M1 dominated by Mg, M2 dominated by Al, M3 dominated again by Mg and both T1 and T2 almost fully occupied by Si. The two tetrahedra do not share any oxygen with each other. The T1 tetrahedron shares all its oxygen atoms with M2 and M3 octahedra, while T2 shares one edge with the M2 site and two oxygen vertices with one vertex of M2 and one vertex of M3. Therefore, jeffbenite can be classified as an orthosilicate. Comparison of our data in Table 3 with those of Finger and Conrad (2000) in their table 3 find no difference concerning bond distances, with identical values for all the crystallographic sites. This also explains why the unit-cell volumes between our sample and that of Finger and Conrad (2000) are very close (difference <0.2%).

Petrological importance of jeffbenite: deep or very deep phase?

The significance of jeffbenite and whether it is a primary phase or the product of retrogression of other mantle phases has been a matter of important debate, and viewpoints have changed as more information has become available. The initial recovery of the phase was as mineral grains (30 to 100 μm across) broken out of diamonds and occurring alongside grains of ferropericlase, MgSi-perovskite (bridgmanite) and CaSi-perovskite (Harte and Harris, 1994; Harris *et al.*, 1997; Harte *et al.*, 1999). This mineral association suggested to the above authors that jeffbenite had a limited stability field in the uppermost lower mantle. However, Harris *et al.* (1997) pointed out that jeffbenite had relatively low density and low cation coordination numbers for a lower mantle phase, and the possibility that the mineral was a retrograde product from another phase was not discounted. Finger and Conrad (2000) suggested, without definitive evidence, that jeffbenite crystallized during the ascent of the host diamond as a retrograde phase. In 1997, McCammon *et al.* measuring, by Mössbauer spectroscopy, the Fe^{3+}/Fe_{tot} content of mineral inclusions in diamonds from São Luiz (Brazil) suggested that jeffbenite could show Fe^{3+}/Fe_{tot} from 20 to 75% and that it, due to its association with ferropericlase and retrogressed enstatite, could be stable in the lower mantle.

Hutchison *et al.* (2001) proposed that jeffbenite in diamond has two mineralogical associations. The type-I association includes ferropericlase [(Mg,Fe)O], olivine [$(Mg,Fe)_2SiO_4$] and jeffbenite and is near the lower-mantle/upper-mantle boundary. The type-III association comprises jeffbenite/majoritic garnet, ferropericlase and $(Mg,Fe)SiO_3$ perovskite (bridgmanite) with Na_2O and Al_2O_3 components and is a lower mantle association, (Gasparik and Hutchison, 2000). In detail, Hutchison *et al.* (2001) reported the chemical composition of two jeffbenites in the diamond BZ243A from Sao Luiz region perfectly matching the analyses in our Table 5. Hutchison *et al.* (2001) agreed with Harris *et al.* (1997) and McCammon *et al.* (1997) about the depth of formation of jeffbenite, close to the boundary between the upper and lower mantle.

Kaminsky *et al.* (2001) reported that jeffbenite coexists with bridgmanite ($MgSiO_3$ perovskite); this mineral always being found retrogressed to enstatite in diamond. However, their supposed jeffbenite [similar to that reported by Harte *et al.* (1999)], which is in contact with bridgmanite, has a TiO_2 content of ~8% (almost double that of all other Ti-bearing jeffbenites) and Al_2O_3 of ~17%.

Brenker *et al.* (2002) reported jeffbenite as symplectitic intergrowths with diopside and olivine and associated in the same diamond with ferropericlase. The diamond studied in that work was from Kankan in Guinea. These authors then suggested that such an association could have a primary origin within the lower mantle but, based on their observations, they stated that jeffbenite could form as a retrograde phase within the transition zone of the Earth's mantle and need not be restricted to the upper part of the lower mantle. They also noted that high Fe^{3+} contents may favour the formation of jeffbenite. The samples studied by Brenker *et al.* (2002) are very similar to the chemical composition of jeffbenite studied in our work.

Hayman *et al.* (2005) investigated 69 alluvial diamonds from Rio Soriso (Juina area). In some of them they found jeffbenite. In detail, in one diamond they found jeffbenite in contact with ferropericlase and in a second diamond in contact with $MgSiO_3$ bridgmanite (assumed primary structure). Mainly based on the TiO_2 content of their jeffbenite (i.e. ~5%), Hayman *et al.* (2005) rejected the retrograde transition zone origin proposed by Brenker *et al.* (2002) in favour of a deeper origin at ~660 km depth, (the lower mantle boundary). The chemical

composition of jeffbenite studied by Hayman *et al.* (2005) shows SiO_2 close to 40%, $TiO_2 \approx 5\%$, $Al_2O_3 \approx 19\%$. Also these authors found no symplectitic textures for touching jeffbenite-ferropericlase and jeffbenite-bridgmanite.

Bulanova *et al.* (2010) studied several diamonds from the Juina region reporting jeffbenite. The chemical analyses of their jeffbenite show low SiO_2 (i.e. ~35%) and Al_2O_3 (~20%), very high FeO (~23%) and TiO_2 (~4%) and very low MgO (~16%). This jeffbenite could contain almost 50% of the Fe-analogue and shows no symplectitic textures. Bulanova *et al.* (2010) suggested that estimates of depth for their sample could only be, by analogy with other previous works, typical of the boundary between the transition zone and lower mantle.

Harte (2010) in his review of mineral inclusions in deep diamonds noted that where experimental data for the transition zone and upper mantle find mineral assemblages containing majoritic garnet, then in the diamond inclusion associations the majoritic garnet often appears to be replaced by jeffbenite. Harte (2010) also suggested that although various interpretations on the occurrence of jeffbenite have been proposed, its capacity to hold ferric iron could represent further evidence of a deep origin, as it was demonstrated that in deep mantle silicates Fe^{3+} is, in general, significantly abundant (McCammon *et al.*, 2004; Frost *et al.*, 2004).

Armstrong and Walter (2012) performed, for the first time, a high pressure-temperature experimental study on jeffbenite synthesis using a laser-heated diamond-anvil-cell. These authors found that the phase assemblage determined by synchrotron X-ray diffraction consisted of jeffbenite + garnet + pseudobrookite + enstatite from 6 to 10 GPa. Using a Ti-rich jeffbenite bulk composition, these authors additionally found that jeffbenite is stable at a maximum pressure of 10–13 GPa at 1300–1700 K. At higher pressures either garnet (to ~20 GPa) or bridgmanite (>~20 GPa) was stable. Based on these results, the authors ruled out direct incorporation of jeffbenite in diamond at the transition zone – lower mantle boundary. Instead, they suggested (1) entrapment as a primary mineral by diamond in the upper mantle; or (2) retrograde formation from a high-pressure garnet or bridgmanite precursor. Armstrong and Walter (2012) proposed that jeffbenite originated as bridgmanite in the lower mantle in mafic protoliths and that it formed upon retrograde conversion at pressures less than ~13 GPa. With only slight reservations Harte and Hudson (2013) accepted the results of Armstrong and Walter (2012), and used a combined garnet-perovskite end-member mineral plot to show how jeffbenite might result from retrograde decomposition of both Al-bearing bridgmanite and majoritic garnet.

Finally, the most recent report of jeffbenite is from Zedgenizov *et al.* (2014), who placed jeffbenite in the transition zone – lower mantle boundary.

In general, all possible compositions of jeffbenites reported so far in the literature are shown in Table 8. Based on this table we can classify jeffbenites in three main compositional ranges: (1) Ti-free and low-Fe jeffbenite; (2) Ti-rich and high-Fe jeffbenites; and (3) Ti-rich and low Fe-jeffbenites. However, for Fe-rich jeffbenites it would be extremely important to analyse them by single-crystal X-ray diffraction to obtain the cation partitioning for Fe and Mg. Indeed, as we have shown in this work (see for example Table 2), the M1 site could host a considerable amount of iron and in the case of very Fe-rich jeffbenites like those found by Bulanova *et al.* (2010) and Thomson *et al.* (2014) we cannot exclude that this site could be dominated by Fe. This would correspond to a new mineral, the Fe-analogue of jeffbenite

Elastic properties of jeffbenite

Unfortunately, so far there are no literature data available for the compressibility and/or thermal expansion of jeffbenite. Such crucial thermodynamic properties could help in obtaining a thermodynamic stability field for different compositions. At the moment, in order to get the volume variation of jeffbenite as a function of pressure we can use the diffraction data in Armstrong and Walter (2012). In their table 4, these authors obtained a unit-cell volume of 783.51 $Å^3$ for their synthetic jeffbenite at room pressure and a volume of 749.02 $Å^3$ at 9.6 GPa. A simple calculation to obtain an indication of bulk modulus, K_T, could be performed applying the following relationship: K_T (GPa) = $\Delta P/(\Delta V/V_0)$. Applying this relationship we obtain K_T = 218 GPa.

Such a value is definitively larger than that of all pyrope-rich garnets ($K_{T,pyrope\text{-}almandine}$ = 164–173 GPa; Milani *et al.*, 2015), majorite (K_T = 160 GPa; Angel *et al.*, 1989) and of other Mg-rich high-pressure silicates like ringwoodite ($K_{T,Mg_2SiO_4\text{-}Fe_2SiO_4}$ = 180–190 GPa; Nestola *et al.*, 2010; Ganskow *et al.*, 2010; Ye *et al.*, 2012), wadsleyite (K_T = 170 GPa; Ye *et al.*, 2010) and oxides like Mg-Fe-Al-Cr spinels ($K_T \approx 185$ GPa; Nestola *et al.*, 2014*b*) and ferropericlase (K_T = 150–160 GPa; Jacobsen *et al.*, 2002). Its bulk

modulus, however, is lower than that of $MgSiO_3$ bridgmanite ($K_T = 253$ GPa; Vanpeteghem *et al.*, 2006), which is the only high-pressure Mg-silicate with a larger bulk modulus than jeffbenite.

Further work on the high-pressure and high-temperature behaviour of jeffbenite is in progress to define its experimental compressibility and thermal expansion.

Conclusions

The only experimentally determined stability field for jeffbenite available so far is that of Armstrong and Walter (2012) and this work provides the maximum pressure at which jeffbenite can be stable, i.e. 13 GPa at 1700 K. Based on the experimental stability field and the absence of jeffbenite from any other geological setting, we are confident that jeffbenite is entrapped in diamond in the deep upper mantle. Thus, in general, we can confirm that jeffbenite is without any doubt a sub-lithospheric mineral.

The results of Armstrong and Walter (2012) considerably affect the suggestions made in earlier work on the *P-T* stability field of jeffbenite, and cast doubt upon its occurrence as a primary phase in the lower part of the transition zone and the uppermost lower mantle. However, the stability field of Armstrong and Walter (2012) is that of a Ti-rich jeffbenite and not a Ti-free jeffbenite like the one investigated here. So, it is important to determine the roles that TiO_2 and also FeO and Fe_2O_3 play in extending the stability field of jeffbenite to higher or lower pressures.

Although these matters require further resolution, at the present time the two main possibilities for the formation of jeffbenite are: (1) entrapment as a primary mineral by diamond in the deepest regions of the upper mantle at pressures up to 10 to 13 GPa (Armstrong and Walter, 2012); (2) retrograde formation from a bridgmanite or high-pressure garnet (majoritic garnet) precursor below 13 GPa (Brenker *et al.*, 2002; Armstrong and Walter, 2012; Harte and Hudson, 2013).

Acknowledgements

This research was supported by the ERC Starting Grant 2012 to FN (agreement no. 307322) and NERC grant NE/J008583/1 to MJW and SCK. We are grateful to Chris Smith and Galina Bulanova for access to the Collier-4 diamond RC2-7. We thank M. Welch and a second anonymous referee for improving the manuscript.

References

Angel, R.J. and Nestola, F. (2015) A century of mineral structures: how well do we know them? *American Mineralogist*, **101**, 1036–1045.

Angel, R.J., Finger, L.W., Hazen, R.M., Kanzaki, M., Weidner, D.J., Liebermann, R.C. and Veblen, D.R. (1989) Structure and twinning of single-crystal $MgSiO_3$ garnet synthesized at 17 GPa and 1800°C. *American Mineralogist*, **74**, 509–512.

Angel, R.J., Mazzucchelli, M.L., Alvaro, M., Nimis, P. and Nestola, F. (2014) Geobarometry from host-inclusion systems: the role of elastic relaxation. *American Mineralogist*, **99**, 2146–214.

Angel, R.J., Alvaro, M., Nestola, F. and Mazzucchelli, M. L. (2015*a*) Diamond thermoelastic properties and implications for determining the pressure of formation of diamond inclusion systems. *Russian Geology and Geophysics*, **56**, 211–220.

Angel, R.J., Nimis, P., Mazzucchelli, M.L., Alvaro, M. and Nestola, F. (2015*b*) How large are departures from lithostatic pressure? Constraints from host-inclusion elasticity. *Journal of Metamorphic Geology*, https://doi.org/10.1111/jmg.12138.

Armstrong, L.S. and Walter, M.J. (2012) Tetragonal almandine pyrope phase (TAPP): retrograde Mg-perovskite from subducted oceanic crust? *European Journal of Mineralogy*, **24**, 587–597.

Barron, L.M., Barron, B.J., Mernagh, T.P. and Birch, W.D. (2008) Ultrahigh pressure macro diamonds from Copeton (New South Wales, Australia), based on Raman spectroscopy of inclusions. *Ore Geology Reviews*, **34**, 76–86.

Brenker, F.E., Stachel, T. and Harris, J.W. (2002) Exhumation of lower mantle inclusions in diamond: A TEM investigation of retrograde phase transitions, reactions and exsolution. *Earth and Planetary Science Letters*, **198**, 1–9.

Bulanova, G.P., Walter, M.J., Smith, C.B., Kohn, S.C., Armstrong, L.S., Blundy, J. and Gobbo, L. (2010) Mineral inclusions in sublithospehric diamonds from Collier 4 kimberlite pipe, Juina, Brazil: subducted protoliths, carbonated melts and primary kimberlite magmatism. *Contributions to Mineralogy and Petrology*, **160**, 489–510.

Chopin, C. (1984) Coesite and pure pyrope in high-grade blueschists of the Western Alps: a first record and some consequences. *Contributions to Mineralogy and Petrology*, **86**, 107–118.

Droop, G.T.R. (1987) A general equation for estimating Fe (super 3+) concentrations in ferromagnesian silicates and oxides from microprobe analyses, using stoichiometric criteria. *Mineralogical Magazine*, **51**, 431–435.

Finger, L.W. and Conrad, P.G. (2000) The crystal structure of "Tetragonal Almandine-Pyrope Phase" (TAPP): a re-examination. *American Mineralogist*, **85**, 1804–1807.

Frost, D.J., Liebske, C., Langenhorst, F., McCammon, C. A., Trunnes, R.G. and Rubie, D.C. (2004) Experimental evidence for the existence of iron-rich metal in the Earth's lower mantle. *Nature*, **428**, 409–412.

Ganskow, G., Ballaran, T.B. and Langenhorst, F. (2010) Effect of iron on the compressibility of hydrous ringwoodite. *American Mineralogist*, **95**, 747–753.

Gasparik, T. and Hutchison, M.T. (2000) Experimental evidence for the origin of two kinds of inclusions in diamonds from the deep mantle. *Earth and Planetary Science Letters*, **181**, 103–114.

Harris, J.W., Hutchison, M.T., Hursthouse, M., Light, M. and Harte, B. (1997) A new tetragonal silicate mineral occurring as inclusions in lower mantle diamonds. *Nature*, **387**, 486–488.

Harte, B. (2010) Diamond formation in the deep mantle: the record of mineral inclusions and their distribution in relation to mantle dehydration zones. *Mineralogical Magazine*, **74**, 189–215.

Harte, B. and Harris, J.W. (1994) Lower mantle mineral associations preserved in diamonds. *Mineralogical Magazine*, **58A**, 384–385.

Harte, B. and Hudson, N.F.C. (2013) Mineral associations in diamonds from the lowermost Upper mantle and uppermost lower mantle. *Proceedings of 10th International Kimberlite Conference*, 235–253.

Harte, B., Harris, J.W., Hutchison, M.T., Watt, G.R. and Wilding, M.C. (1999) Lower mantle mineral associations in diamonds from Sao Luiz, Brazil. Pp. 125–153 in: *Mantle Petrology: Field Observations and High Pressure Experimentation: A Tribute to Francis R. (Joe) Boyd* (Y. Fei, C.M. Bertka and B.O. Mysen, editors). The Geochemical Society, Houston, Texas, USA.

Hayman, P.C., Kopylova, M.G. and Kaminsky, F.V. (2005) Lower mantle diamonds from Rio Soriso (Juina area, Mato Grosso, Brazil). *Contributions to Mineralogy and Petrology*, **149**, 430–445.

Holland, T.J.B. and Redfern, S.A.T. (1997) Unit cell refinement from powder diffraction data: The use of regression diagnostics. *Mineralogical Magazine*, **61**, 65–77.

Howell, D., Wood, I.G., Nestola, F., Nimis, P. and Nasdala, L. (2012) Inclusions under remnant pressure in diamond: a multi-technique approach. *European Journal of Mineralogy*, **24**, 563–573.

Hutchison, M.T., Hursthouse, M.B. and Light, M.E. (2001) Mineral inclusions in diamonds: associations and chemical distinctions around the 670-km discontinuity. *Contributions to Mineralogy and Petrology*, **142**, 199–126.

Jochum, K.P., Willbold, M., Raczek, I., Stoll, B. and Herwig, K. (2005) Chemical characterisation of the USGS reference glasses GSA-1G, GSC-1G, GSD-1G, GSE-1G, BCR-2G, BHVO-2G and BIR-1G using EPMA, ID-TIMS, ID-ICP-MS and LA-ICP-MS. *Geostandards and Geoanalytical Research*, **29**, 285–302.

Jacobsen, S.D., Spetzler, H.A., Reichmann, H.J., Smyth, J.R., Mackwell, S.J., Angel, R.J. and Bassett, W.A. (2002) Gigahertz ultrasonic interferometry at high P and T: new tools for obtaining a thermodynamic equation of state. *Journal of Physics – Condensed Matter*, **14**, 11525–11530.

Kaminsky, F. (2012) Mineralogy of the lower mantle: a review of "super-deep" mineral inclusions in diamond. *Earth Science Reviews*, **110**, 127–147.

Kaminsky, F.V., Zakharchenko, O.D., Davies, R., Griffin, W.L., Khachatryan-Blinova, G.K. and Shiryaev, A.A. (2001) Superdeep diamonds from the Juina area, Mato Grosso State, Brazil. *Contributions to Mineralogy and Petrology*, **140**, 734–753.

Kolesov, B.A. and Geiger, C.A. (1998) Raman spectra of silicate garnets. *Physics and Chemistry of Minerals*, **25**, 142–151.

Lafuente, B., Downs, R.T., Yang, H. and Stone, N. (2015) The power of databases: the RRUFF project. Pp. 1–30 in: *Highlights in Mineralogical Crystallography* (T. Armbruster and R.M. Danisi, edtors). De Gruyter, Berlin, Germany.

Liou, J.G., Zhang, R.Y., Liu, F.L., Zhang, Z.M. and Ernst, W.G. (2012) Mineralogy, petrology, U-Pb geochronology, and geologic evolution of the Dabie-Sulu classic ultrahigh-pressure terrane, East-Central China. *American Mineralogist*, **97**, 1533–1543.

Mandarino, J.A. (1981) The Gladstone-Dale relationship: Part IV. The compatibility concept and its application. *The Canadian Mineralogist*, **19**, 441–450.

McCammon, C., Hutchison, M. and Harris, J. (1997) Ferric iron content of mineral inclusions in diamonds from São Luiz: a view into the lower mantle. *Science*, **278**, 434–436.

McCammon, C.A., Stachel, T. and Harris, J.W. (2004) Iron oxidation state in lower mantle mineral assemblages. II. Inclusions in diamonds from Kankan, Guinea. *Earth and Planetary Science Letters*, **222**, 423–434.

Milani, S., Nestola, F., Alvaro, M., Pasqual, D., Mazzucchelli, M.L., Domeneghetti, M.C. and Geiger, C.A. (2015) Diamond-garnet geobarometry: the role of garnet compressibility and expansivity. *Lithos*, **227**, 140–147.

Nestola, F. and Smyth, J.R. (2016) Diamonds and water in the deep Earth: a new scenario. *International Geology Review*, **58**, 263–276.

Nestola, F., Nimis, P., Angel, R.J., Milani, S., Bruno, M., Prencipe, M. and Harris, J.W. (2014*a*) Olivine with diamond-imposed morphology included in diamonds. Syngenesis or protogenesis? *International Geology Review*, **56**, 1658–1667.

Nestola, F., Periotto, B., Andreozzi, G.B., Bruschini, E. and Bosi, F. (2014*b*) Pressure-volume equation of state for chromite and magnesiochromite: a single-crystal X-ray diffraction investigation. *American Mineralogist*, **99**, 1248–1255.

Nestola, F., Boffa Ballaran, T., Koch-Mueller, M., Balic-Zunic, T., Taran, M., Olsen, L., Princivalle, F., Secco, L. and Lundegaard, L. (2010) New accurate compression data for gamma-Fe_2SiO_4. *Physics of the Earth and Planetary Interiors*, **183**, 421–425.

Parkinson, C.D. (2000) Coesite inclusions and prograde compositional zonation of garnet in whiteschist of the HP-UHPM Kokchetav massif, Kazakhstan: a record of progressive UHP metamorphism. *Lithos*, **52**, 215–233.

Sheldrick, G.M. (2008) A short history of SHELX. *Acta Crystallographica Section A*, **64**, 112–122.

Stachel, T. (2001) Diamonds from the asthenosphere and the transition zone. *European Journal of Mineralogy*, **13**, 883–892.

Thomson, A.R., Kohn, S.C., Bulanova, G.P., Smith, C.B., Araujo, D. and Walter, M.J. (2014) Origin of sub-lithospheric diamonds from the Juina-5 kimberlite (Brazil): constraints from carbon isotopes and inclusion compositions. *Contributions to Mineralogy and Petrology*, **168**, article 1081.

van Roermund, H.L.M. and Drury, M.R. (1998) Ultrahigh pressure (P > 6 GPa) garnet peridotites in Western Norway: exhumation of mantle rocks from >185 km depth. *Terra Nova*, **10**, 295–301.

Vanpeteghem, C.B., Zhao, J., Angel, R.J., Ross, N.L. and Bolfan-Casanova, N. (2006) Crystal structure and equation of state of $MgSiO_3$ perovskite. *Geophysical Research Letters*, **33**, L03306.

Walter, M.J., Kohn, S.C., Araujo, D., Bulanova, G.P., Smith, C.B., Gaillou, E., Wang, J., Steele, A. and Shirey, S.B. (2011) Deep mantle cycling of oceanic crust: evidence from diamonds and their mineral inclusions. *Science*, **334**, 54–57.

Ye, Y., Smyth, J.R., Hushur, A., Manghnani, M.H., Lonappan, D., Dera, P. and Frost, D.J. (2010) Crystal structure of hydrous wadsleyite with 2.8% H_2O and compressibility to 60 GPa. *American Mineralogist*, **95**, 1765–1772.

Ye, Y., Brown, D.A., Smyth, J.R., Panero, W.R., Jacobsen, S.D., Chang, Y.Y., Townsend, J.P., Thomas, S.M., Hauri, E.H., Dera, P. and Frost, D.J. (2012) Compressibility and thermal expansion of hydrous ringwoodite with 2.5(3) wt% H_2O. *American Mineralogist*, **97**, 573–582.

Zedgenizov, D.A., Kagi, H., Shatsky, V.S. and Ragozin, A.L. (2014) Local variations of carbon isotope composition in diamonds from Sao-Luis (Brazil): Evidence for heterogenous carbon reservoir in sub-lithospheric mantle. *Chemical Geology*, **363**, 114–124.

Zhang, L.F., Ellis, D.J. and Jiang, W.B. (2002) Ultrahigh-pressure metamorphism in western Tianshan, China: Part I. Evidence from inclusions of coesite pseudomorphs in garnet and from quartz exsolution lamellae in omphacite in eclogites. *American Mineralogist*, **87**, 853–860.